

A UAS PLATFORM FOR ASSESSING SPECTRAL, STRUCTURAL, AND THERMAL PATTERNS OF ARCTIC TUNDRA VEGETATION

Ran Meng^{1,2*}, Dedi Yang², Andrew McMahon², Wouter Hantson³, Dan Hayes³, Amy Breen⁴, Shawn Serbin²

¹Huazhong Agriculture University, ²Brookhaven National Laboratory, ³University of Maine, ⁴University of Alaska Fairbanks

*Corresponding author, E-mail: mengran@mail.hzau.edu.cn

ABSTRACT

As climate continues to warm, detailed geospatial spectral, structural, and thermal information, related to water, carbon, and energy cycling, are required for modeling the future state of the Arctic biome. To address these needs we have developed a cost-effective, multi-sensor UAS-based remote sensing platform for acquiring high resolution spectral, structural, and thermal measurements of Arctic vegetation. We successfully deployed this remote sensing platform in three sites along an elevation gradient near Nome, Alaska in summer 2017. Corresponding workflows have been further developed for assessing spectral, structural, and thermal patterns of arctic tundra biomes from the collected datasets. Our results demonstrate that the UAS platform can successfully (1) map heterogenous vegetation composition and (2) assess corresponding spectral, structural, and thermal patterns of Arctic tundra biomes. This study not only presents a novel and innovative approach for collecting high resolution spectral, structural and thermal information for characterizing Arctic tundra biome patterns, but also a basis for informing the modeling of climate feedbacks between the biosphere and the atmosphere in response to ongoing global change.

Index Terms—plant traits, vegetation composition, object-oriented classification, spectroscopy, thermal infrared

1. INTRODUCTION

A number of studies have documented dramatic changes in the composition, distribution, and functioning of Arctic tundra vegetation, in particular, in response to ongoing global change over the past several decades [1, 2]. These changes can lead to numerous biochemical and biophysical consequences (i.e., changes to carbon and nutrient storage and cycling), with complex feedbacks [3]. Methods for measuring detailed spectral, structural, and thermal properties of Arctic tundra vegetation, related to water, carbon, and energy cycling (e.g., functional traits, albedo, land surface temperature), are thus crucial for modeling and

projecting the future state of Arctic biome, as climate continues to warm [4].

The recent development of Unmanned Aircraft System (UAS)-based remote sensing platforms have provided the opportunity to fill a critical gap in the scaling between field measurements and satellite remote sensing observations. These platforms allow the characterization of Arctic vegetation at unprecedented high spatial-temporal resolution for improving our understanding of Arctic vegetation biodiversity and dynamics [5]. For example, consumer-grade cameras on UAS platforms have been used successfully to characterize optical features of vegetation and topography at centimeter-level spatial resolution [6]; UAS-acquired overlap RGB imagery and its generated dense point clouds with computer vision algorithms (i.e., Structure from Motion, SfM) can be used to derive three dimensional (3D) structural features of diverse vegetation in remote regions [7]. Additionally, thermal infrared (TIR) cameras suitable for UAS platform can be used to conduct spatially diagnostic assessment of vegetation health and stress [8].

To meet the geospatial measurement needs in Arctic tundra biomes we assembled a small UAS-based remote sensing platform with multiple off-the-shelf (OTS) sensors including optical RGB, spectroscopic (i.e. “hyperspectral”), and TIR sensors and integrated information extraction pipelines. The aim of this study was two-fold: first, to confirm that UAS-based platform provides a viable alternative to traditional field surveys for detecting spectral, structural and thermal patterns in Arctic tundra biomes. Second, to provide a roadmap for utilizing UAS-based very high-resolution data collection platform to examine vegetation compositions and corresponding spectral, structural, thermal patterns in Arctic tundra biomes.

2. MATERIALS AND METHODS

2.1 Study area and data collections

An octocopter, model CarbonCore Cortex Heavy Lift (Autonomous Avionics, Colorado, USA), was used as the platform to carry the sensor suite and perform all flights (Fig.2). The octocopter UAS has an integrated survey-grade

Global Navigation and an inertial motion unit (IMU) for navigation and error corrections associated with pitch, roll, and heading. The octocopter carried our customized sensor suite (Fig.2) including a TIR camera (ICI 9640 P-Series), a RGB camera (Canon EOS M6), and two visible-near-infrared (VNIR) spectrometers (Ocean Optics flame series).

The ICI TIR camera has a pixel resolution of 640x480, 14 bit dynamic range, and a 7 μ m -14 μ m spectral band with 30mm manual focus lens (20° x 15° Field of View, FOV). Canon EOS M6 is a 24MP mirrorless CMOS camera with 15-45mm lens. The Ocean Optic flame spectrometer has a spectral region of 350–1000 nm at a 1.5 nm spectral resolution and a 16-bit radiometric resolution.

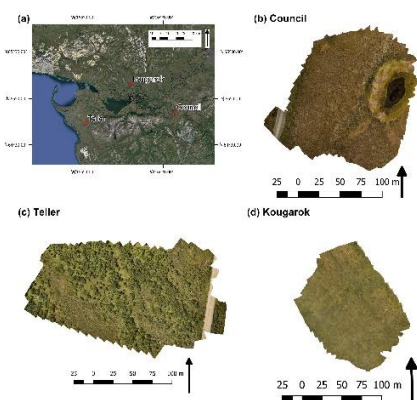


Fig. 1 Locations of study area and UAS-collected ortho-imagery showing the landscapes of study areas by different flight missions

To minimize issues related to variable light conditions in the Arctic, we utilized a dual Ocean Optics FLAME spectrometer setup where the upward spectrometer measuring downwelling radiance was fitted with a cosine-corrector (~180° FOV) while the downward spectrometer measuring upwelling radiance from the surface was fitted with a variable FOV lens; we set this lens to 14° FOV. To reduce vibration effects during the aerial surveys, both Canon EOS M6 and ICI TIR camera were mounted on a 3-axis gimbal (GREMSY H3) attached to the bottom of UAS platform on a vibration dampening plate. We further developed a software infrastructure called the Modular Data Collection System (MoDaCS), to link UAS mission planning and flight control to the sensor suite, enabling automated data acquisition synced with customizable flight plans and monitored in real time (if desired) or completely autonomous (Andrew et al., in preparation).



Fig. 2 UAS-based remote sensing platform

Nine successful UAS-flights were successfully conducted covering regions about 168,000 m² ground areas (Fig.1) during the period of July 27th to August 8th 2017. During each flight, we deployed 5 or more ground control points (GCPs) across the survey region for image georeferencing. We recorded the coordinates of GCPs, using a hand-held decimeter-level differential global positioning system (DGPS, Trimble Geo7x). After post-processing, the final registration error was less than 10 cm. To validate the spectra quality collected by the UAS-based remote sensing platform, we also collected near-surface spectra across the study site using a Spectra Vista HR-1024i spectrometer.

2.2 UAS-collected data processing

To produce high quality ortho-imagery and 3D point clouds, we mosaicked and georeferenced the UAS-collected RGB imagery using the SfM algorithm in Agisoft PhotoScan software (referred to Agisoft later) with the collected GCPs [5]. Agisoft can reduce image artifacts caused by camera angle and altitude changes during the UAS flights. The point clouds generated from Agisoft were processed into Digital Surface Models (DSMs), followed by vegetation canopy height models (CHMs) generated by subtracting lowest ground point of cloud points at each five-meter grid from the generated DSMs (Fig.3).

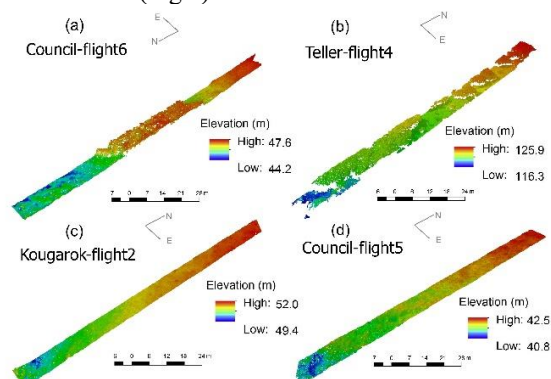


Fig.3 Surface-from-Motion (SfM)-generated DTM cloud points

Post-processing of the UAS-collected TIR imagery was done using the same workflow of RGB imagery; however, because of coarse spatial resolution of TIR imagery and low contrast in our study area, some of direct SfM-based TIR imagery strip mosaicking was not successful. As such we applied another semi-automatic method for mosaicking and georeferencing the left TIR imagery from aerial surveys with the help of ENVI software. Specifically, we first determined the rough image center coordinate of each single TIR imagery using the GPS and IMU data including altitude, flight direction, and time stamps, which are acquired from the MoDaCS; then we georeferenced and mosaicked the single TIR imagery in ENVI software, with the help of corresponding RGB ortho-images. Regarding the UAS-

collected spectra, we calculated the footprint and location of each measurement according to the GPS, IMU and data logging information from the MoDaCS.

2.3 Vegetation composition classification

RGB ortho-imagery were segmented into image objects using the multi-resolution segmentation algorithm (scale = 15, shape = 0) in eCognition software. During the segmentation process, the minimum object areas were defined as 10 cm² (10 pixels) using only RGB information. Classification predictors listed in Table 1 were then calculated based on the segmentation results. The classification legend was determined according to the local major plant functional types (PFTs), including 11 land cover types: Sedge Moss (SM), Willow Birch Tundra (WBT), Mixed Dwarf Shrub and Red Moss (MDSRM), Mixed Dwarf Shrub and White Lichen (MDSWL), Wet Graminoid (WG), Dead Sege or Moss (DSM), Waterbody (WB), Tussock Tundra Health (TTH), Shadow and Dark Cryptogams (SDC), White Lichen (WL), Road and Soil (RS).

Table 1 Variables used for vegetation classification

Variable	Description
Red\Green Blue_mean_max_min_std	Mean, max, minimum and standard deviation of red, green, blue channel value
NDGB_mean_max_min_std	Mean, max, minimum and standard deviation of Normalized difference of Green and Blue channel value: $G-B/G+B$
NDGR_mean_max_min_std	Mean, max, minimum and standard deviation of Normalized difference of Green and Red channel value: $G-R/G+R$
Mean_vegetation_height	Mean vegetation height derived from CHM
Compactness	$(Object_length \text{ by } Object_width) / Area$
Texture_mean_max_min_std	Mean, max, minimum and standard deviation of grey level co-occurrence texture

Representative Region Of Interests (ROIs) for each classification type were selected directly from the 1cm RGB SfM-generated ortho-imagery based on *in-situ* photos and expert knowledge. A stratified sampling scheme was applied to split the ROIs into 60% and 40% for classification training and validation, respectively. Finally, the Random Forests (RF) algorithm was applied for vegetation composition classification in R. We chose RF because it is a widely used non-parametric classification algorithm, making no assumption about the distribution of predictor variables [9].

2.4 Characterizing spectral and thermal traits of major vegetation types

To characterize the spectral traits, we calculated the Normalized Difference Vegetation Index (NDVI), using all the UAS-based spectrometer measurements. We then overlaid NDVI measurement on the RGB ortho-imagery generated before. To characterize the plant thermal traits, we first overlaid the vegetation composition map with the thermal canopy temperature imagery. Then to reduce computation task, we randomly extracted three thousand objects from 10 major vegetation types. Mean object-level thermal temperature values were calculated for each random selected object based on the thermal temperature imagery. Similarly, boxplots of mean thermal temperature by 10 plant function type were generated to examine the thermal temperature differences.

3. RESULTS AND DISCUSSTION

Our UAS-based remote sensing platform successfully collected three types of remote sensing datasets across the study area, providing detailed information on vegetation spectrum, TIR, and structure at the centimeter level. At one of the Council study sites, the vegetation community demonstrated dramatic differences in spectral and thermal signatures across the wetness gradient from the road edge to a thaw pond (Fig.4). The hyperspectral-derived normalized difference vegetation index (NDVI) also varied with locations and changes in vegetation type (Fig.4): Wet Graminoid areas had the highest values, while Shadow areas were lowest. The SfM-generated point clouds successfully characterized the vegetation structure at different sites, useful for feature for vegetation composition classification (Fig.3).

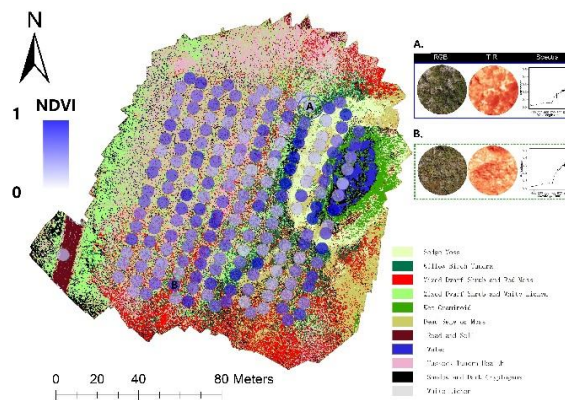


Fig.4 Vegetation composition map and overlaid hyperspectral-derived NDVI values within each footprint; subplot A and B show two examples of footprint-level RGB ortho-imagery and corresponding TIR temperature and hyperspectral measurement

TTH were dominant at road edges (dry areas); WG and SM can be easily found around water pond (wet areas); some dead or dry sedge moss can be found at the relatively “dry” areas of water pond (Fig.4). This phenomenon indicates that the water dynamics has strong effects on local vegetation status and composition, in accordance with previous studies [3].

In addition, our results indicated that the object-level canopy temperatures also changed with vegetation composition types and could be used as important features for studying plant traits (Fig.5): WG has the lowest canopy temperature in general because of waterbody effects; on the contrary, WL has the highest canopy temperature because of low transpiration and water content.

The shape of UAS-collected spectra matched with field-measured spectra in general, but showed a relative lower magnitude in both visible and NIR regions (Fig.6). This phenomenon could be likely explained by the fact the stronger scattering effects by UAS remote sensing platform at higher altitude, comparing to that of near-surface spectra measurements by field spectrometer [4]. The confusion matrix (not list here) showed that the overall accuracy of vegetation composition classification is 84.54% with the User’s accuracy between 54.13% (DSM) and 96.48% (RS) and Producer’s accuracy between 59.80% (DSM) and 98.80% (RS).

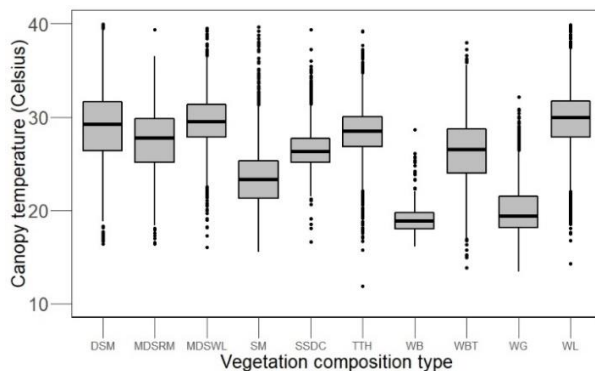


Fig.5 Boxplots of object-level canopy temperature by vegetation composition type; Refer to Section 2.3 for acronyms

4.CONCLUSIONS

The recent development of UAS technology is facilitating a transformational change in the remote sensing of Arctic tundra biomes. Here we present a cost-effective UAS platform for remote sensing of arctic tundra biomes based on off-the-shelf instrumentations. Our results indicate that the UAS-based remote sensing platform can provide spectral, structural, and thermal measurements at unprecedented scales with greater flexibility than manned aircraft, thereby greatly advancing our capability for monitoring and projecting Arctic tundra biomes in response to ongoing global change.

5. ACKNOWLEDGMENT

This work was supported by the Next-Generation Ecosystem Experiments (NGEE Arctic) project that is supported by the Office of Biological and Environmental Research in the United States Department of Energy, Office of Science, and through the Department of Energy contract No. DE-SC0012704 to Brookhaven National Laboratory.

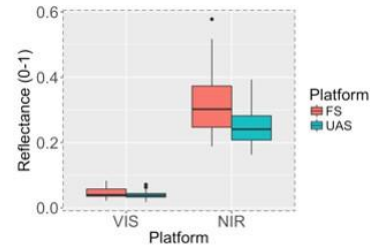


Fig.6 Boxplots of Visible (VIS) and Near-infrared (NIR) reflectance measured by UAS and field spectrometer platform

6. REFERENCES

- [1] S. J. Goetz, A. G. Bunn, G. J. Fiske, and R. A. Houghton, "Satellite-observed photosynthetic trends across boreal North America associated with climate and fire disturbance," *Proceedings of the National Academy of Sciences of the United States of America*, vol. 102, no. 38, pp. 13521-13525, Sep 2005.
- [2] S. Gauthier, P. Bernier, T. Kuuluvainen, A. Shvidenko, and D. Schepaschenko, "Boreal forest health and global change," *Science*, vol. 349, no. 6250, pp. 819-822, Aug 2015.
- [3] I. H. Myers-Smith et al., "Shrub expansion in tundra ecosystems: dynamics, impacts and research priorities," *Environmental Research Letters*, vol. 6, no. 4, p. 045509, Dec 2011.
- [4] N. Liu, P. Budkewitsch, and P. Treitz, "Examining spectral reflectance features related to Arctic percent vegetation cover: Implications for hyperspectral remote sensing of Arctic tundra," *Remote Sensing of Environment*, vol. 192, pp. 58-72, Apr 2017.
- [5] I. Colomina and P. Molina, "Unmanned aerial systems for photogrammetry and remote sensing: A review," *ISPRS Journal of Photogrammetry and Remote Sensing*, vol. 92, no. 0, pp. 79-97, Jun 2014.
- [6] J. P. Dash, M. S. Watt, G. D. Pearse, M. Heaphy, and H. S. Dungey, "Assessing very high resolution UAV imagery for monitoring forest health during a simulated disease outbreak," *ISPRS Journal of Photogrammetry and Remote Sensing*, vol. 131, pp. 1-14, Sep 2017.
- [7] J. P. Dandois and E. C. Ellis, "High spatial resolution three-dimensional mapping of vegetation spectral dynamics using computer vision," *Remote Sensing of Environment*, vol. 136, pp. 259-276, Sep 2013.
- [8] J. A. J. Berni, P. J. Zarco-Tejada, L. Suárez, and E. Fereres, "Thermal and narrowband multispectral remote sensing for vegetation monitoring from an unmanned aerial vehicle," *IEEE Transactions on Geoscience and Remote Sensing*, vol. 47, no. 3, pp. 722-738, Feb 2009, Art no. 4781575.
- [9] R. Meng et al., "Detection of tamarisk defoliation by the Northern Tamarisk Beetle based on multitemporal Landsat 5 Thematic Mapper imagery," *GIScience & Remote Sensing*, vol. 49, no. 4, pp. 510-537, May 2012.